Regional CBF Changes in Parkinsoni¦s Disease: A Correlation with Motor Dysfunction

Journal:	*European Journal of Nuclear Medicine and Molecular Imaging*
Manuscript ID:	EJNM-06-0421.R1
Manuscript Type:	Original Article
Date Submitted by the Author:	24-Nov-2006
Complete List of Authors:	Hsu, Jung-Lung; Shin Kong Wu Ho-Su Memorial Hospital, Neurology; Taipei Medical University, Graduate Institute of Medical Informatics; The Salk Institute, Computational Neurobiology Lab Jung, Tzyy-Ping; The Salk Institute, Computational Neurobiology Lab; University of California, Institute for Neural Computation Hsu, Chien-Yeh; Taipei Medical University, Graduate Institute of Medical Informatics Hsu, Wei-Chih; Shin Kong Wu Ho-Su Memorial Hospital, Department of Neurology Chen, Yen-Kung; Shin Kong Wu Ho-Su Memorial Hospital, Departments of Nuclear Medicine and PET Center Duann, Jeng-Ren; The Salk Institute, Computational Neurobiology Lab; University of California, Institute for Neural Computation Wang, Han-Cheng; Shin Kong Wu Ho-Su Memorial Hospital, Department of Neurology Makeig, Scott; The Salk Institute, Computational Neurobiology Lab; University of California, Institute for Neural Computation
Keywords:	Parkinson's disease, SPECT, regional cerebral blood flow, independent component analysis, statistical parametric mapping

Regional CBF Changes in Parkinson's Disease: A Correlation with Motor Dysfunction

Running head line: ICA of SPECT data in Parkinson's disease

Jung-Lung Hsu[1,2,4], M.D.; Tzyy-Ping Jung[4,5], PhD; Chien-Yeh Hsu[2], PhD; Wei-Chih Hsu[1], M.D.; Yen-Kung Chen[3], M.D.,PhD; Jeng-Ren Duann[4,5], PhD; Han-Cheng Wang[1], M.D.; Scott Makeig[4,5], PhD

1 Department of Neurology, Shin Kong Wu Ho-Su Memorial Hospital, Taipei, Taiwan
2 Graduate Institute of Medical Informatics, Taipei Medical University, Taipei, Taiwan
3 Departments of Nuclear Medicine and PET Center, Shin Kong Wu Ho-Su Memorial Hospital, Taipei, Taiwan
4 Computational Neurobiology Lab, the Salk Institute, La Jolla, CA 92037-5800, USA
5 Institute for Neural Computation, University of California, San Diego, CA 92093

Corresponding author: Han-Cheng Wang
Department of Neurology,
Shin Kong Wu Ho-Su Memorial Hospital
95, Wen Chang Road, Shih Lin District,
Taipei, Taiwan.
Tel: 886-2-28332211 (ext 2593)
Fax: 886-2-28344906
E-mail: drhan@ms1.hinet.net

First author: Jung-Lung Hsu
Department of Neurology, 95 Wen Chang Rd, Shih Lin, Taipei, Taiwan
Tel: 886-2-28332211 (ext 2598)
Fax: 886-2-28344906
Email: tulu@ms36.hinet.net

Word count of manuscript: 4085 words

ABSTRACT

Purpose: The purpose of this study is to further localize cerebral perfusion abnormalities, and to better correlate these abnormalities with the clinical severity of Parkinson's disease (PD).

Methods: A single photon emission computerized tomography (SPECT) study was performed on 27 patients with PD and 24 aged-matched controls. SPECT images were spatially normalized, concatenated, and then decomposed using infomax independent component analysis (ICA). The resulting image components were separated by logistic regression into two subspaces: "disease-related" components whose subject weights differed between groups, and "disease-unrelated" components. The resultant regional cerebral blood flow (rCBF) subspace images were normalized to global CBF for each subject, and then processed in SPM to compare rCBF values between PD and control subjects.

Results: In the "disease-related" image subspace, patients with PD exhibited significantly higher adjusted rCBF in the putamen, globus pallidum, thalamus, brainstem and the anterior lobe of the cerebellum, and significant hypoperfusion in the pariteo-occipital cortex, dorsolateral prefrontal, and in the insula and cingulate gyrus. The motor Unified Parkinson's Disease Rating Scale (UPDRS) scores correlated negatively with rCBF in the insula and cingulate gyrus. In the "disease-unrelated" image subspace, no brain voxels exhibited a significant group difference.

Conclusions: ICA-based separation of normalized images into "disease-related" and "disease-unrelated" subspaces revealed many disease-related group blood flow differences. The regions revealed by ICA are consistent with the current model of PD. These rCBF changes in PD have not been fully demonstrated in any single functional imaging study previously.

Key words: SPECT, Parkinson's disease, regional cerebral blood flow, independent component analysis, statistical parametric mapping,

Introduction

Parkinson's disease (PD) is a common neurodegenerative disease with four cardinal motor features: resting tremor, bradykinesia, cogwheel rigidity and postural instability. The pathophysiological mechanisms of PD remain largely unknown, but the primary neurotransmitter deficit appears to be the loss of dopaminergic (DA) nigrostriatal neurons in substantia nigra pars compacta [1], resulting in a loss of brain dopamine, most prominently in the striatum. According to the basal ganglia circuit model of PD [2, 3], the loss of dopaminergic innervation results in abnormal activities in the globus pallidus (GPi). These abnormal activities contribute directly and indirectly to the movement abnormalities observed in PD. Although the correlations between motor features and their cerebral substrates are not yet completely understood, a common expectation is that the alteration of functional activity in the basal ganglia in PD patients should be associated with changes in regional cerebral metabolism (rCMR) and regional cerebral blood flow (rCBF) in certain brain areas.

^{99m}Tc-HMPAO single photon emission computerized tomography (SPECT) is a well-established method of assessing rCBF. SPECT data have been analyzed utilizing either Region Of Interest (ROI) analysis [4], which investigates blood flow abnormalities in predefined regions, or Statistical Parametric Mapping (SPM), which can generate images of blood flow abnormalities for each voxel in the whole brain image. Results of previous reports regarding rCBF differences between PD patients and controls have been mixed. In the basal ganglia, for example, rCBF has been reported to be reduced [5], increased [6, 7] or unchanged [8]. Recently, results by Imon et al. [9] showed that stage 1 or 2 PD patients had adjusted rCBF increases in bilateral putamen and the right hippocampus, while stage 3 or 4 patients had increases in bilateral putamen, globus pallidus, hippocampus, cerebellar hemispheres (dentate nuclei), left ventrolateral thalamus, right insula, and right inferior temporal gyrus.

As is now widely acknowledged, functional nueroimaging analyzing methods utilizing model-driven approaches, such as SPM, are largely univariate and depend on some hypotheses on the data they are dealing with. There are complementary methods using data-driven approaches, such as principle component anlaysis (PCA), clustering analysis and blind source separation, which are multivariate. These multivariate approaches have contributed greatly to studies on disease-related changes in patterns of functional connectivity [10,11]. In a recent study, PCA was utilized on FDG-PET data combined with multivariate network analysis at group level. The results from that approach can serve as an indicator of PD severity that is better than the univariate approaches [10].

Independent component analysis (ICA), also a multivariate approach, is a recently

developed data-driven approach to imaging data analysis [12]. It has been widely applied to the analyses of functional neuroimaging data, including electroencephalography (EEG), magnetoencephalography (MEG), event-related potential (ERP), functional magnetic resonance imaging (fMRI) [13], and other biomedical signals. ICA methods had effectively separated artifact components from fMRI data [14]. The present study uses ICA to remove the disease-unrelated SPECT activity including artifacts and rCBF unaffected by PD. Voxel-based statistic parametric mapping (SPM) is then applied for analysis. This novel approach would hopefully reveal more areas of significant rCBF changes with better clinical correlation in PD patients.

Materials and methods

Subjects

Twenty-seven PD patients and twenty-four age-matched control subjects participated in this study. Patients were diagnosed with PD according to the research diagnostic criteria of Ward and Gibb [15]. Hoehn and Yahr method was used for disease staging. [16]. The PD patients (21 male, 6 female; mean age 65.6 $\pm$ 10 years) were divided into three groups: 6 at Hoehn-Yahr stage 1, 10 at stage 2, and 11 at stage 3. Patients' motor symptoms were clinically evaluated using the motor part of Unified Parkinson's Disease RatingS cale (UPDRS) prior to the SPECT study [17]. The patients had been maintained on stable anti parkinsonian therapy with optimal clinical benefit for at least one month before the study. Medications included various combinations of L-DOPA with decarboxylase inhibitor (carbidopa), dopamine agonists, anticholinergic agents, and amantadine hydrochloride. Twenty-four control subjects (8 male, 16 female; mean age 61.8 $\pm$ 9 years) were healthy volunteers without major neurologic or psychiatric disorder (including alcoholism, substance abuse, head trauma with consciousness loss or cerebral vascular disorder). All subjects were given information about the procedure and had given signed informed consent prior to participating in the study.

Experimental Protocol

Each patient was instructed to fast for 12 hours before the SPECT imaging, in the hope of inducing an "off" state. Patients and control subjects were injected with 740MBq (20 mCi) of ^{99m}Tc-HMPAO 30 minutes prior to scanning. Scanning was performed parallel to the canthomeatal line using a dual-head Gamma Camera VariCam (GE, USA) with high resolution collimator (full width half maximum: 8 mm). A polycarbonate head holder was used to reduce head movement during scanning. The acquisition parameters were 120

projections recorded in step-and-shoot mode over a 360° rotation arch. For each head, 60 projections were acquired. The angular step size was 3° and the frame rate was 25 seconds per step. Each acquisition was completed in 30 minutes. The acquisition matrix was 128x128; zoom, 1.5. The reconstruction of SPECT images was achieved using a filtered back projection algorithm with a Metz filter of power 3, resulting in 80 contiguous 128x128 transaxial image slices with in-plane resolution of 1.77x1.77 mm and slice thickness of 1.8 mm. Attenuation correction based on Chang's method [18] was performed on each slice, with a uniform attenuation coefficient of 0.11.

Image Analysis

All images were first converted to Analyze format from their native image format using MRIcro software (http://www.psychology.nottingham.ac.uk/staff/crl/mricro.html) developed by Chris Rorden. Each individual SPECT image was then re-oriented and spatially normalized to the standard Montreal National Institute (MNI) template included in SPM2 (http://www.fil.ion.ucl.ac.uk/spm/) using a 12-parameter affine transformation. Non-linear SPM algorithms (7x8x7, 12 non-linear iterations with moderate nonlinear regularization) were used to spatially normalize each subject's image to the SPM SPECT template. As a result, each subject's image was re-sampled into 2x2x2 mm voxels in a cube with axes right-left, anterior-posterior, and superior-inferior, respectively. After spatial normalization, the individual SPECT images from normal controls (1-24) and patients (25-51) were concatenated, forming a SPECT data matrix, X, with 51 rows (the number of subjects) and 79*95*69 columns (the total number of voxels).

Independent Component Analysis

ICA decomposition was performed within Matlab (The MathWorks, Inc) under FMRLAB developed by Duann et al. (http://sccn.ucsd.edu/fmrlab) [19]. Within FMRLAB, the off-brain voxels were first removed using an image intensity threshold selected interactively through a graphic user interface. Then, the Bell-Sejnowski information-maximization (Infomax) algorithm [12], as implemented by Makeig et al. [20], was used to derive maximally spatially independent components of the 51 collected images. Applied to our SPECT data matrix, X, ICA found an 'unmixing' matrix, W, that decomposed or linearly unmixed the concatenated SPECT data into a sum of spatially independent components, $U = W \times X$, where U was a matrix of spatially fixed independent component SPECT images. Each subject's weight in the column of inverted W matrix represents the relative adjusted rCBF effects in each subject image of the component on the brain regions. After ICA training converged, a logistic regression was applied to the subject weights for

each column, using a probability threshold of $p < 0.05$, to find "disease-related" components exhibiting a significant weight difference between patients (columns 25-51) and controls (columns 1-24). The remaining components were considered "disease-unrelated" components. Components in these two subspaces were separately back-projected and summed to reconstruct the disease-related and unrelated portions or subspaces of the individual subject images.

Statistic analysis

SPM analysis was performed on both the reconstructed "disease-related" and "disease-unrelated" portions pre-processed by the ICA method described above. In each portion, a 3-D Gaussian filter (16 mm width) was used to smooth each image. The mean CBF of each image was scaled to 50 for each subject.

In both portions, between-group comparisons (controls and PD) were performed on a voxel-by-voxel basis using as general linear model based on the theory of Gaussian fields [21,22] within SPM. The first comparison sought areas of increased perfusion, and the second, areas of decreased perfusion in PD. The resulting set of voxel values for each comparison constituted a statistical parametric map or SPM{t}. The SPM{t} value were thresholded at the $p < 0.001$ uncorrected ($t = 3.27$) level; the number and size of connected clusters of suprathreshold voxels were recorded. Corrected (for multiple non-independent comparsions) cluster-level p values were calculated for each cluster based on their spatial extent [20]. Clusters with a corrected p value less than 0.01, which yield > 100 voxels, were considered significant. SPM results were then overlaid on a normalized MR image.

Finally, we tested for brain areas in which the ICA-adjusted rCBF changes were correlated with the motor-UPDRS score using the SPM (single-subject, covariant-only) method. Data from back projection of the "disease-related" components set constituted 27 PD subject images. The motor UPDRS score was used as a covariant to look for score-related regions. In this study, voxel clusters threshold above a significance threshold set at $p < 0.003$ uncorrected ($t = 3.00$) level and an extent threshold set at corrected p value less than 0.01 were considered significant.

Results

Table 1 shows the demographic and clinical distribution of the subjects. There was no significant difference in age between controls and patients. In the ICA preprocessed data, 9 components were classified by logistic regression as "disease-related" and 42 components as "disease-unrelated".

Significant effects of PD-related changes were extensive in the ICA preprocessed data.

In the "disease-related' component set, PD patients showed increased adjusted rCBF (hyperperfusion) in the bilateral putamen and globus pallidus, ventral lateral nucleus of thalamus, brainstem, cerebellum, precentral gyrus, superior frontal cortex, middle occipital gyrus as well as hypoperfusion in the bilateral middle frontal gyrus (dorsolateral prefrontal cortex), parieto-occipital cortex, superior temporal cortex, insular and anteriorcingulate gyrus. Details of the brain areas involved on the ICA preprocessed data are given in table 2 and 3, and figure 1. By contrast, in the "disease-unrelated" component subspace, not a single brain area showed significantly disease-related changes of adjusted rCBF.

In patients, analysis of the "disease-related" ICA subspace data showed that ICA-adjusted rCBF in the bilateral anteriorcingulated, cingulated gyrus and postcentral gyrus, parahippocampus gyrus, right insula, and right inferior parietal lobulewere negatively correlated with motor UPDRS scores(figure 2). No region showed positive correlation with motor UPDRS scores. Details of these results are shown in table 4.

Discussion

By first applying spatial ICA to eliminate disease-unrelated signal change variability, and then using SPM to assess the statistical significance, we were able to observe adjusted rCBF changes between groups. In the "disease-related" data subspace, many brain areas showed significant ICA-adjusted rCBF group differences, including hypoperfusion in the supplementary motor area and hyperperfusion in various basal ganglion nuclei. By contrast, in the complementary "disease-unrelated" subspace, no significant group difference existed. The findings are consistent with predictions from the basal ganglia circuit model of PD [2, 3]. These results demonstrate that image preprocessing using ICA can further separate "disease-related" from "disease-unrelated" signal changes in SPECT images and improve study results.

ICA-adjusted rCBF increases in PD

We found that in PD, the adjusted rCBF is increased in the basal ganglia, thalamus, brainstem, and cerebellum. Among these regions, an increased adjusted rCBF in the bilateral putamen, globus pallidum, thalamus, and pons is to be expected according to the basal ganglia circuit model [2, 3]. It is also consistent with findings from previous studies using SPECT and FDG-PET [9, 23]. Our findings of increased ICA-adjusted CBF in the globus pallidum and thalamus are also in agreement with the facts that surgical ablation or deep brain stimulation to these regions improves clinical symptoms in PD [24, 25]. This may imply that neuronal hyperactivity in these regions, reflected as hypermetabolism in this study, is responsible for parkinsonian symptoms. Increased ICA-adjusted rCBF in the putamen may

result from more complex feedback mechanisms primarily induced by striatal dopamine deficiency [26]. Results from previous SPECT and FDG-PET studies regarding cerebellar blood flow have been contradictory. The increased cerebellar rCBF found in our study agrees with some previous reports [9] including that of Hilker et al. [27], who found a relatively increased left rostral cerebellar rCMR in advanced PD patients prior to surgery. In another FDG and F-dopa PET study, Ghaemi et al. [28] also found cerebellar metabolic hyperactivity in PD, which is more closely related to akinesia and rigidity rather than to tremor. However, our results did not show any correlation between motor UPDRS scores and cerebellum hyperperfusion. We did not further divide the motor UPDRS scores into akinesia, rigidity, and tremor subcategories to correlate each symptom with metabolic changes. We think the motor UPDRS scores, by its nature only semi-quantitative, may not be a reliable clinical indicator if further divided.

Our patients also showed a relatively hyperperfusion in the middle and inferior temporal and fusiform gyri. It may be related to the anti-parkinsonian treatment these patients were receiving, since medication and deep brain stimulation can both activateregions including the temporal gyri [29]. Nonpsychotic visual hallucinations in PD may also be associated with hyperperfusion in the right temporal gyrus and hypoperfusion in the fusiform gyrus, as reported by Oishi et al. [30].

ICA-adjusted rCBF decreases in PD

There was a widely distributed decrease in ICA-adjusted rCBF in the cerebral cortex of Parkinsonian patients. Involved regions included posterior parieto-occipital cortex, precuneus, cingulate, insula, inferior frontal, dorsolateral prefrontal cortex, and supplementary motor cortex. In addition, the caudate and medial dorsal nucleus of the thalamus also showed decreases in ICA-adjusted rCBF.

Firbank et al. [31] and Antonini et al [32], using SPECT to study PD patients with cognitive impairment, both found that demented PD patients had significant perfusion decrements in all the cortical areas, particularly in temporal and parietal regions. Another factor that may be responsible for decreased rCBF in parieto-temporal cortex is autonomic failure. Arahata et al. [33] reported that rCMR in the cerebral cortex in PD with autonomic failure was markedly reduced, particularly in occipital cortex, inferior parietal and superior parietal cortex.

Our patients showed a relatively hypoperfusion in the inferior frontal cortex. Hypometabolism in inferior frontal cortex has been reported in advanced PD and in PD with depression by FDG-PET study [34, 35]. The observed abnormalities in these brain regions are probably more related to neuropsychiatric symptoms in PD [36].

We also found hypoperfusion in insular and bilateral cingulate cortex. Various rCBF changes (increases [9] or decreases [23]) in the insula have been reported in PD. Most PET and SPECT studies have not reported decreased of rCMR or rCBF in the cingulate gyrus. In a SPECT study on PD patients treated with deep-brain stimulation to the subthalamic nucleus (STN), Sestini et al [37] demonstrated a significant stimulation-induced rCBF increase in the right pre-supplementary motor area (pre-SMA), anterior cingulate cortex, dorsolateral prefrontal cortex, and medial Brodmann's Area 8. Their results provide direct evidence of the association between the basal ganglia circuit and the limbic system, and imply that hypoperfusion in these areas may account for an impairment of thehigher -order aspects of motor control. Thus insula and cingulate hypoperfusion in PD in the present study is more consistent with the extended predictions of the basal ganglia circuit model.

ICA-adjusted rCBF correlates with the motor UPDRS scores

We found a negative correlation between the motor UPDRS scores and the ICA-adjusted rCBF in the bilateral cingulated, anterior cingulated, postcentral gyrus, right inferior parietal lobule, insula and fusiform gyrus. Previous studies correlating PD neural substrate with ratings of clinical symptoms had produced inconsistent results [23, 38, 39]. It may be due to the fact that these studies were carried out using different imaging techniques (e.g. PET vs. SPECT) and different clinical evaluating tools. Hypoperfusion in the cingulate gyrus had been shown to relate to PD with predominant postural instability and gait difficulty. [40]. Studies utilizing either univariate or multivariate methods did find a UPDRS score correlation with insular activites, but not with cingulate activities [10,23]. Our results not only demonstrated a hypoperfusion in anteriorcingulate , cingulate gyrus and insula regions, but also a negative correlation of perfusion in these regions with motor UPDRS scores. This may suggest thatboth insula and cingulate hypoperfusion should have a relation with disease severity, and participate in motor performance. Our findings of a negative correlation between motor UPDRS and therCMR in inferior parietal cortex, and primary associate visual cortex, were supported by the findings of others [23,39]. These results demonstrate that the abnormally decreased perfusion in specific cortical regions are quantitatively related to the severity of Parkinson's disease.

Conclusions

In the present study, we assessed adjusted rCBF differences between PD patients and normal controls using independent component analysis (ICA) as a data processing tool. The ICA-adjusted rCBF changes in various brain areas found by this method were compatible with the standard pathophysiological model of PD. Our data also showed a hypoperfusion in

the insula and cingulated gyrus in PD that is negatively correlated with motor UPDRS scores. We think ICA preprocessing is a useful complement for purely hypothesis-driven methods of analyzing group SPECT data differences. This method might be useful in developing alternative and/or more comprehensive disease and brain circuit models for PD or other neurodegenerative diseases.

Acknowledgement

This study was sponsored by the Shin Kong Wu Ho-Su Memorial Hospital (SKH 8302-95-DR-16).

REFERENCES

1. Hornykiewcz O. Dopamine (3-hydroxytyramine) and brain function. Pharmacol Rev. 1966;18:925-64.
2. Albin RL, Young AB, Penney JB. The functional anatomy of basal ganglia disorders. Trends Neurosci. 1989;12:366-75.
3. Alexander GE, Crutcher MD. Functional architecture of basal ganglia circuits: neural substrates of parallel processing. Trends Neurosci. 1990;13:266-71.
4. Holman BL, Johnson KA, Gerada B, Carvalho PA, Satlin A. The scintigraphic appearance of Alzheimer's disease: a prospective study using technetium-99m-HMPAO SPECT. J. Nucl. Med. 1992;32:181–85.
5. Perlmutter JS, Raichle ME. Regional blood flow in hemiparkinsonism. Neurology. 1985;35:1127-34.
6. Henriksen L, Boas J. Regional cerebral blood flow in hemiparkinsonian patients: emission computerized tompgraphy of inhaled 133Xenon before and after levodopar. Acta Neurol Scand. 1985;71:257-66.
7. Wolfson LI, Leenders KL, Brown LL, Jones T. Alterations of cerebral blood flow and oxygen metabolism in Parkinson's disease. Neurology 1985;35:1399-1405.
8. Pizzolato G, Dam M, Borsato N, et al. (99mTc)-HMPAO SPECT in Parkinson's disease. J Cereb Blood Flow Metab. 1988;8(suppl):S101-8.
9. Imon Y, Matsuda H, Ogawa M, Kogure D, Sunohara N. SPECT image analysis using statistical parametric mapping in patients with Parkinson's disease. J Nucl Med. 1999;40;1583-89.
10. Vaasinen V, Maguire RP, Hundemer HP, Leenders KL. Corticostriatal covariance patterns of 6-[F18]fluoro-L-dopa and [F18]fluorodeoxyglucose PET in Parkinson's disease. J Neurol. 2006;253:340-8.
11. Dujardin K, Defebvre L, Duhamel A, Lecouffe P, Rogelet P, Steinling M, Destee A. Cognitive and SPECT characteristics predict progression of Parkinson's disease in newly diagnosed patients. J Neurol. 2004;251:1383-92.
12. Bell AJ, Sejnowski TJ. An information-maximization approach to blind separation and blind deconvolution. Neural Comput. 1995;7(6):1129-59.
13. Jung T-P, Makeig S, McKeown M.J., Bell, A.J., Lee T-W, and Sejnowski TJ. Imaging Brain Dynamics Using Independent Component Analysis, Proceedings of the IEEE, 2001;89:1107-22.
14. McKeown MJ, Makeig S, Brown GG, Jung T-P, Kindermann SS, and Sejnowski TJ. Analysis of fMRI by Blind Separation into Independent Spatial Components. Human Brain Mapping. 1988;6:160-88.
15. Ward CD, Gibb WR. Research Diagnostic Criteria for Parkinson's disease. In Streifler M, Korczyn AD, Melamed E, Youdim MBH (eds). Advances in Neurology. 1990;53,245-49.
16. Hoehn MM, Yahr MD. Parkinsonism: onset, progression and mortality. Neurology. 1967;17:427-42.
17. Fahn S. Elton RL, Members of the UPDRS Development Committee. Unified Parkinson's disease and movement disorders. In Recent Developments in Parkinson's disease vol2., Fahn S, Marsden CD, Calne DB, Goldstein M eds., Florham Park, NJ Mcmillan Health Care Information, pp. 153-164, 1987.
18. Chang LT. A method for attenuation correction in radionuclide computed

tomography. IEEE Trans Nucl Sci. 1978;25:638-43.
19. Duann JR, Jung TP, Kuo WJ, Yeh TC, Makeig S, Hsieh JC, Sejnowski TJ. Single-trial variability in event-related BOLD signals. Neuroimage. 2002;15:823-35
20. Makeig S, Jung TP, Bell AJ, Ghahremani D, Sejnowski TJ. Blind separation of auditory event-related brain responses into independent components. Proc Natl Acad Sci U S A. 1997;94:10979-84.
21. Friston KJ, Frith CD, Liddle PF, Frackowiak RSJ. Comparing functional (PET) images: the assessment of significant change. J Cereb Blood Flow Metab. 1991;11:690-99.
22. Friston KJ, Worsley KJ, Frackowiak RSJ, Mazziotta JC, Evans AC. Assessing the significance of focal activations using their spatial extent. Hum Brain Mapping. 1994;1:214-20.
23. Kikuchi A, Takeda A, Kimpara T, et al. Hypoperfusion in the supplementary motor area, dorsolateral prefrontal cortex and insular cortex in Parkinson's disease. J Neurol Sci. 2001;193:29-36.
24. Dogali M, Fazzini E, Kolodny E, et al. Stereotactic ventral pallidotomy for Parkinson's disease. Neurology. 1995;45:753-61.
25. Alvarez L, Macias R, Lopez G, et al. Bilateral subthalamotomy in Parkinson's disease: initial and long-term response. Brain. 2005;128:570-83.
26. Antonini A, Vontobel P, Psylla M, et al. Complememtary positron emsission tomographic studies of the striatal dopaminergic system in Parkinson's disease. Arch Neurol. 1995;52:1183-90.
27. Hilker R, Voges J, Weisenbach S, et al. Subthalamic nucleus stimulation restores glucose metabolism in associative and limbic cortices and in cerebellum: evidence from a FDG-PET study in advanced Parkinson's disease. J Cereb Blood Flow Metab. 2004;24:7-16.
28. Ghaemi M, Raethjen J, Hilker R, et al. Monosymptomatic resting tremor and Parkinson's disease: A multitracer positron emission tomographic study. Mov Disord 2002;17:782-8.
29. Goerendt IK, Lawrence AD, Mehta MA, Stern JS, Odin P, Brooks DJ. Distributed neural actions of anti-parkinsonian therapies as revealed by PET. J Neural Transm. 2006;113:75-86.
30. Oishi N, udaka F, Kameyama M, Sawamoto N, Hashikawa K, Fukuyama H. Regional cerebral flow in Parkinson disease with nonpsychotic visual hallucinations. Neurology 2005;65:1708-15.
31. Firbank MJ, Colloby SJ, Burn DJ, McKeith IG, O'Brien JT. Regional cerebral blood flow in Parkinson's disease with and without dementia. Neuroimage. 2003;20:1309-19.
32. Antonini A, De Notaris R, Benti R, De Gaspari D, Pezzoli G. Perfusion ECD/SPECT in the characterization of cognitive deficits in Parkinson's disease. Neurol Sci. 2001;22:47-8.
33. Arahata Y, Hirayama M, Ieda T, et al. Parieto-occipital glucose hypometabolism in Parkinson's disease with autonomic failure. J Neurol Sci.1999;163:119-26.
34. Mayberg HS, Starkstein SE, Sadzot B, et al. Selective hypometabolism in the inferior frontal lobe in depressed patients with Parkinson's disease. Ann Neurol. 1990;28:57-64.

35. Berding G, Odin P, Brooks DJ, et al. Resting regional cerebral glucose metabolism in advanced Parkinson's disease studied in the off and on conditions with ((18)F)FDG-PET. Mov Disord. 2001;16:1014-22.
36. Black KJ, Hershey T, Hartlein JM, Carl JL, Perlmutter JS. Levodopa Challenge Neuroimaging of Levodopa-Related Mood Fluctuations in Parkinson's Disease. Neuropsychopharmacology. 2005;30:590-601.
37. Sestini S, Scotto di Luzio A, Ammannati F, et al. Changes in regional cerebral blood flow caused by deep-brain stimulation of the subthalamic nucleus in Parkinson's disease. J Nucl Med. 2002;43:725-32.
38. Lozza C, Marie RM, Baron JC. The metabolic substrates of bradykinesia and tremor in uncomplicated Parkinson's disease. Neuroimage. 2002;17:688-99.
39. Nagano-Saito A, Kato T, Arahata Y, et al. Cognitive- and motor-related regions in Parkinson's disease: FDOPA and FDG PET studies. Neuroimage. 2004;22:553-61.
40. Mito Y, Yoshida K, Yabe I, Makino K, Tashiro K, Kikuchi S, Sasaki H. Brain SPECT analysis by 3D-SSP and phenotype of Parkinson's disease. J Neurol Sci. 2006;241:67-72.

TABEL 1
Demography and UPDRS Scores of PD and Controls

	Controls	PD patients			P value*
		H&Y stage I	H&Y stage II	H&Y stage III	
Number	24	6	10	11	
Age†	61.8 ± 9	62.3 ± 11	63.1 ± 13	69.6 ± 6	NS‡
Sex (M/F)	8 / 16	2 / 4	8 / 2	11 / 0	< 0.05
Motor UPDRS		21.8 ± 4	24.5 ± 9	29.4 ± 8	NS§

*: P value: compares controls to all PD patients.

†: Mean ± SD

‡: NS: not significant.

§: post-hoc analysis between H&Y stage I-III was not significant.

TABLE 2

Basal Ganglion, Cerebellum and Brain Stem Areas Showing Significant Adjusted CBF Difference Between PD and Controls in "Disease-Related Components" Subspace.

Structural name	Voxel size[#]	Peak Z value	MNI coordinates (mm)			State
			X	Y	Z	
Basal ganglion						
Caudate Head (L)	35	4.77	-6	4	6	-
Caudate Head (R)	75	5.22	4	4	6	-
Putamen (L)	559	6.99	-26	-14	2	+
Putamen (R)	145	5.16	28	-18	12	+
Lateral Globus Pallidus (L)	169	7.77	-24	-16	-2	+
Lateral Globus Pallidus (R)	55	4.59	24	-16	4	+
Medial Globus Pallidus (L)	41	6.42	-20	-10	-2	+
Thalamic nucleus						
Medial Dorsal Nucleus (R)	58	3.98	6	-22	12	-
Ventral Lateral Nucleus (L)	62	6.29	-18	-16	10	+
Ventral Posterior Lateral Nucleus (L)	45	7.37	-20	-22	2	+
Cerebellum						
Culmen (L)	1035	6.48	-26	-50	-18	+
Culmen (R)	1111	6.63	10	-54	-12	+
Declive (L)	764	6.27	-24	-54	-16	+
Declive (R)	487	6.17	10	-56	-16	+
Dentate (L)	203	5.48	-10	-46	-34	+
Dentate (R)	201	4.66	14	-48	-26	+
Fastigium (L)	53	4.64	-8	-48	-28	+
Fastigium (R)	42	4.42	6	-48	-26	+
Anterior Lobe (L)	1707	6.57	-4	-40	-36	+
Anterior Lobe (R)	1744	6.62	10	-54	-12	+
Brain stem						
Midbrain (L)	292	6.28	-2	-32	-14	+
Midbrain (R)	243	6.08	2	-32	-14	+
Pons (L)	618	7.22	-8	-34	-34	+
Pons (R)	536	6.48	4	-28	-32	+
Medulla (L)	131	6.30	-6	-36	-44	+
Medulla (R)	105	5.84	2	-38	-44	+

[*]: State, +: adjusted CBF in PD higher than controls', -: adjusted CBF in PD lower than controls'; L/R: left side and right side.

[#]: voxel size: $8mm^3$

TABLE 3

Brain Areas Showing Significant Adjusted CBF Difference Between PD and Controls in "Disease-Related Components" Subspace.

Structural name	BA‡	Voxel size#	Peak Z value	MNI coordinates (mm)			State
				X	Y	Z	
Limbic lobe							
Insula (L)	13	559	7.45	-36	-30	18	-
Insula (R)	13	352	4.66	58	-32	20	-
Anterior Cingulate (L)	32	297	5.53	-8	38	28	-
Anterior Cingulate (R)	32	405	5.70	6	38	28	-
Cingulate Gyrus (L)	24	1435	6.29	-2	-30	44	-
Cingulate Gyrus (R)	24	1551	6.30	2	-10	46	-
Posterior Cingulate (L)	30	743	7.90	-10	-66	14	-
Posterior Cingulate (R)	30	548	7.49	12	-70	14	-
Frontal lobe							
Superior Frontal Gyrus (L)	9	77	4.79	-20	56	36	+
Superior Frontal Gyrus (R)	9	170	5.39	16	60	36	+
Medial Frontal Gyrus (L)	8	151	6.36	-4	44	44	-
Medial Frontal Gyrus (R)	8	124	5.64	2	42	44	-
Medial Frontal Gyrus (L) †	24	284	5.99	-4	-10	48	-
Medial Frontal Gyrus (L)	10	230	6.84	-8	64	18	-
Medial Frontal Gyrus (R)	10	168	7.17	4	68	12	-
Middle Frontal Gyrus (L)	10	181	5.02	-36	38	14	-
Middle Frontal Gyrus (R)	8	193	5.96	36	20	50	-
Inferior Frontal Gyrus (L)	46	207	6.48	-58	36	8	-
Inferior Frontal Gyrus (R)	47	351	5.53	52	38	-10	+
Orbital Gyrus (R)	47	120	5.11	16	26	-28	+
Precentral Gyrus (L)	6	362	5.81	-26	-18	58	+
Precentral Gyrus (R)	4	201	6.40	34	-24	66	+
Parietal lobe							
Postcentral Gyrus (L)	1	48	5.73	-56	-28	44	-
Postcentral Gyrus (L)	2	113	7.20	-58	-30	46	-
Postcentral Gyrus (L)	3	51	5.71	-58	-26	44	-
Postcentral Gyrus (R)	1	43	7.34	66	-22	36	-
Postcentral Gyrus (R)	2	94	7.02	66	-22	32	-
Postcentral Gyrus (R)	3	88	7.51	62	-18	32	-
Inferior Parietal Lobule (L)	40	575	7.14	-62	-40	44	-
Inferior Parietal Lobule (R)	40	540	6.91	68	-26	24	-
Superior Parietal Lobule (L)	7	275	6.28	-38	-60	58	-
Precuneus (L)	31	551	7.96	-8	-68	16	-
Precuneus (R)	31	539	7.79	10	-72	16	-
Angular Gyrus (L)	39	290	7.49	-50	-66	30	-
Occipital lobe							
Middle Occipital Gyrus (L)	19	124	4.69	-48	-84	12	+
Middle Occipital Gyrus (R)	19	432	6.00	54	-70	6	+
Cuneus (L)	18	358	7.47	-2	-74	16	-
Cuneus (R)	18	394	7.71	12	-72	16	-

Temporal lobe							
Superior Temporal Gyrus (L)	38	419	6.29	-50	20	-28	-
Superior Temporal Gyrus (R)	22	133	5.02	38	-56	20	-
Middle Temporal Gyrus (L)	19	97	4.46	-52	-82	14	+
Middle Temporal Gyrus (R)	39	975	6.54	54	-682	10	+
Inferior Temporal Gyrus (L)	20	242	6.29	-34	-2	-50	+
Inferior Temporal Gyrus (R)	20	289	4.42	50	-16	-36	+
Fusiform Gyrus (L)	37	41	4.42	-56	-50	-22	+
Fusiform Gyrus (R)	37	49	5.31	38	-54	-16	+
Parahippocampal Gyrus (L)	36	85	4.96	-32	-30	-26	-

*: State, +: adjusted CBF in PD higher than controls', -: adjusted CBF in PD lower than controls'; L/R: left side and right side.

†: SMA: supplementary motor area.

‡: BA: brodmann area.

#: voxel size: $8mm^3$

TABLE 4

Brain Areas Showing Significant Correlation with Motor UPDRS Scores

Structural Name	BA‡	Voxel size#	Peak Z value	MNI coordinations (mm)		
Negative correlations				X	Y	Z
Cingulate Gyrus (L)	24	72	4.19	-2	8	30
Cingulate Gyrus (R)	31	89	4.69	14	-32	44
Anterior Cingulate (L)	33	44	5.74	-6	10	24
Anterior Cingulate (R)	24	36	4.70	4	14	28
Insula (R)	13	97	5.11	42	-32	18
Precentral Gyrus (L)	4	101	4.10	-56	-14	32
Inferior Parietal Lobule (R)	40	242	6.00	46	-34	34
Postcentral Gyrus (L)	43	78	3.71	-56	-16	34
Postcentral Gyrus (R)	2	215	5.91	48	-32	38
Superior Temporal Gyrus (R)	29	457	5.57	40	-32	16
Fusiform Gyrus (R)	20	92	5.15	54	-20	-28
Parahippocampal Gyrus (L)	36	145	6.14	-26	-16	-32
Uncus(L)	28	51	4.40	-16	2	-30
Pons (L)		45	4.45	-10	-12	-32

L/R: left side and right side.

‡: BA: brodmann area.

#: voxel size: $8mm^3$

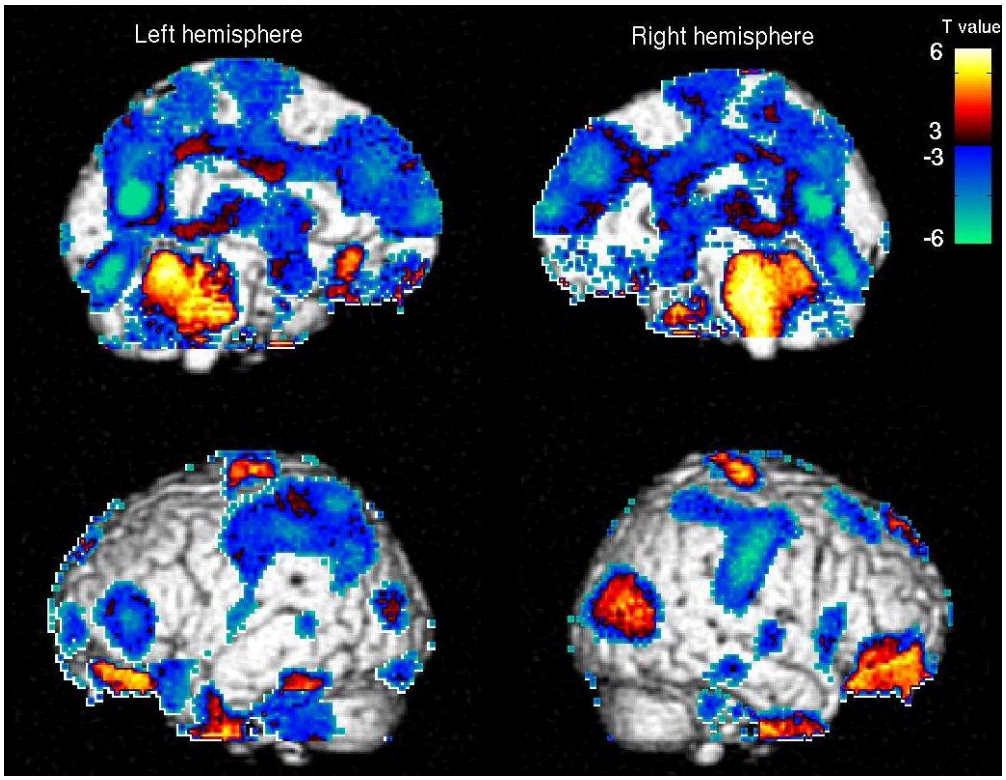

Figure 1. Maximum intensity projection on 3-D rendered brain showing SPM group difference results after ICA pre-processing. Highlighted brain areas show significant ICA-adjusted rCBF changes in Parkinsoni¦s disease compared to normal controls. Results plotted on a 3-D rendered brain template from SPM2. Warm color represents hyperperfusion and cold color, hypoperfusion of ICA-adjusted rCBF in PD. T value represents the severity of rCBF changes.

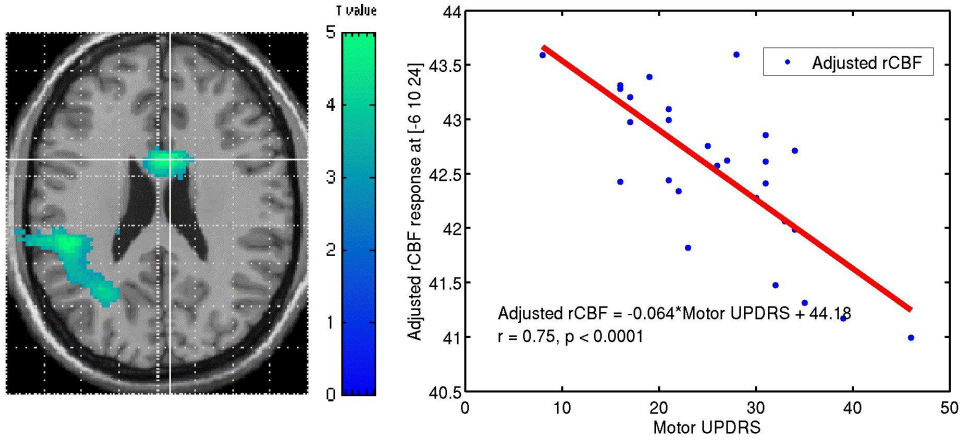

Figure 2. Correlations between motor UPDRS scores and adjusted rCBF. Adjusted rCBF in the left anterior cingulated gyrus was negatively correlated with motor UPDRS scores (r = 0.75).